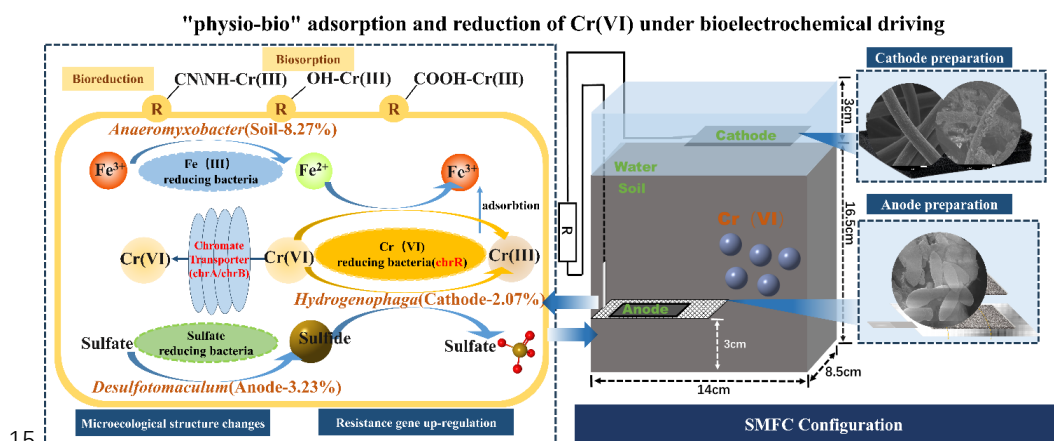




14 **Abstract figure:**



15

16

17 **Abstract:** Microbial fuel cell (MFC) is an efficient in-situ approach to combat pollutants and generate
 18 electricity. This study constructed a soil MFC (SMFC) to reduce Cr(VI) in paddy soil and investigate its
 19 influence on microbial community and microbial resistance characteristics. Fe₃O₄ nanoparticle as the
 20 cathodic catalyst effectively boosted power generation (0.97 V, 102.0 mW/m²), whose porous structure
 21 and reducibility also contributed to Cr reduction and immobilization. After 30 days, 93.67% of Cr(VI)
 22 was eliminated. The bioavailable Cr decreased by 97.44% while the residual form increased by 88.89%.
 23 SMFC operation greatly changed soil enzymatic activity and microbial structure, with exoelectrogens
 24 like *Desulfotomaculum* (3.32% in anode) and Cr(VI)-reducing bacteria like *Hydrogenophaga* (2.07% in
 25 cathode) more than 1000 folds of soil. In particular, SMFC operation significantly enhanced the
 26 abundance of heavy metal resistance genes (HRGs). Among them, *chrA*, *chrB*, and *chrR* increased by
 27 99.54~3314.34% in SMFC anode than control, probably attributed to the enrichment of potential
 28 tolerators like *Acinetobacter*, *Limnohabitans*, and *Desulfotomaculum*. These key taxa were positively
 29 correlated with HRGs but negatively correlated with pH, EC, and Cr(VI), which could have driven Cr(VI)



30 reduction. This study provided novel evidence for bioelectrochemical system application in contaminated

31 paddy soil, which could be a potential approach for environmental remediation and detoxification.

32 **Keywords:** Chromium; Microbial fuel cell; Microbial response; Metal resistance

33



Nomenclature	
SMFC	Soil microbial fuel cell
HRGs	Heavy metal resistance genes
HMs	Heavy metals
HGT	Horizontal gene transfer
EABs	Electrochemical active bacteria
GF	Graphite felt
ORR	Oxygen reduction reaction
WCV	Working circuit voltage
OCV	Open circuit voltage
ARGs	Antibiotic resistance genes
CMFC-A	Anode of the closed circuit group
OMFC-A	Anode of the open circuit group
CMFC-C	Cathode of the closed circuit group
OMFC-C	Cathode of the open circuit group
CMFC-S	Soil of the closed circuit group
OMFC-S	Soil of the open circuit group
NMFC-S	Soil of the non-electrode control group

34 1. Introduction

35 Chromium (Cr) is one of the main toxic heavy metals (HMs), which enters the environment mainly
36 due to its wide use in electroplating, tanning, and other industries (Coetzee et al., 2020). Mineral-sourced
37 phosphate fertilizer also contains high-level Cr, further promoting its spreading and migration in soil and
38 underground water (Chen et al., 2022a). Even a sub-dose of Cr (especially the Cr(VI) state) can promote
39 plasmid-mediated horizontal gene transfer (HGT) (Zhang et al., 2018), causing enrichment of heavy
40 metal resistance genes (HRGs), threatening environmental safety (Guo et al., 2021; Wang et al., 2023a;
41 Wang et al., 2023b; Wang et al., 2020a). Due to the cross-resistant effect of HMs and antibiotics, the
42 enrichment of HRGs and tolerators under Cr exposure has become an emerging concern.

43 Common remediation methods for Cr-influenced soil include chemical reduction and leaching
44 (Cong et al., 2022), electrokinetic remediation (Morales-Benítez et al., 2023), and phytoaccumulation
45 (Yaashikaa et al., 2022), which convert Cr(VI) into insoluble and low toxic forms (e.g., Cr(III)) by
46 adsorption, ion exchange, and redox (Rani et al., 2022). Among them, the microbial approach using
47 functional microbes is commonly used for the continuous treatment of soil-groundwater, which has a



48 low cost without side effects (Fan et al., 2023). However, pollutants can be tightly adsorbed by soil
49 particles and persistently remain (Wang et al., 2023a). The complex soil constituents and competition of
50 indigenous microorganisms inhibit the colonization and development of functional microbes and limit
51 their effectiveness (Guo et al., 2021).

52 Microbial fuel cell (MFC) technology can transform or immobilize HMs and generate electricity
53 utilizing electrochemical active bacteria (EABs) (Chen et al., 2022b; Gupta et al., 2023), which have
54 been used in sediment or soil to treat HMs and organics and monitor environmental toxicity (Li et al.,
55 2023b). At present, soil MFC (SMFC) has been used for pollution control, focusing on pollutant content
56 and forms as well as the electrochemical properties (Hamdan and Salam, 2023; Liu et al., 2023a). There
57 is a lack of systematic research about the MFC effect on soil microbial community structure shifting and
58 resistance characteristics.

59 In this study, an SMFC was constructed to remediate Cr(VI) contaminated paddy soil. EABs were
60 pre-loaded on the SMFC anode to promote electricity production and Cr transformation. Ferroferric
61 oxide (Fe_3O_4) nanoparticles, which can reduce and fix Cr(VI) directly, were used as a catalyst for
62 cathodic oxygen reduction reaction (ORR) (Liu et al., 2023b). During operation, Cr(VI) was reduced and
63 immobilized by bio-physical adsorption and electrochemical-microbial reduction, simultaneously. The
64 Cr(VI) reduction mechanism was comprehensively studied along with the analysis of microbial
65 community structure shaping and HRG variation. For the first time, SMFC-driven Cr(VI) reduction was
66 associated with microbial resistance, which evolved along with microbial adaption and development.
67 This study not only provides a reference for the microbial remediation of polluted soil but also improves
68 the practical field application of MFC.



69 **2. Materials and Methods**

70 **2.1. Chemicals**

71 All the chemicals and reagents were analytical grade or premium pure from Kelong Chemical
72 Reagent Factory, Chengdu, China.

73 **2.2 Construction of SMFC**

74 2.2.1 Soil

75 Paddy soil from Jintang County, Chengdu, China (30°74' N, 104°59' W) was collected and used to
76 construct SMFC. The soil has organic matter, organic carbon, and total nitrogen of 8.84±0.02%,
77 1.74±0.01%, and 321.67±1.25 mg/kg, respectively. Potassium dichromate was added to the soil to
78 achieve a final Cr(VI) concentration of 118.8 mg/kg before use.

79 2.2.2 Electrodes Preparation

80 Aluminum foam (66.0×54.0×5.0 mm) (SANZHENG Metal material, Chengdu, China) was used
81 as anode. The anode microflora was derived from municipal sludge (Chengdu Sixth Sewage Treatment
82 Plant, China) after acclimating with 100 mg/L Cr(VI). Before assembling, the aluminum foam was
83 cultivated in the anode microflora for 2 weeks. Then the anode was tied to titanium mesh tightly with
84 titanium wire. Graphite felt (GF) (100.0×50.0×3.0 mm) was used as the cathode (Table S1). Before
85 use, it was cleaned, dried, and loaded with Fe₃O₄ as the ORR catalyst, as detailed in section 1 of the
86 supplementary material. For characterization, we utilized a scanning electron microscope (SEM) to
87 examine the structure and morphology of the electrode surface. In addition, we performed X-ray
88 photoelectron spectroscopy (XPS) and energy dispersive spectroscopy (EDS) to analyze the valence state



89 and element composition. The phase composition was determined using an X-ray diffractometer (XRD).

90 2.2.3 SMFC construction

91 A plastic box (140.0×85.0×165.0 mm) was used as the SMFC reactor, with 1.50 kg soil and
92 overlying water of 3.0 cm to simulate the flooded state during rice planting. The cathode was floated on
93 the water surface while the anode was buried (about 3.0 cm from the bottom). The cathode and anode
94 were connected to a 2000 Ω resistor using titanium wire. The water level was kept constant by daily
95 replenishment.

96 2.3 Design and Operation

97 Three treatments were set up as shown in Fig. S1. Three parallel was set for each group.

98 1. NMFC: The control group with no electrode. It only contains an equal amount of overlying water
99 and paddy soil.

100 2. OMFC: The open circuit group with disconnected electrodes and equal amounts of overlying
101 water and paddy soil.

102 3. CMFC: The complete closed-circuit SMFC capable of producing electricity, with electrodes
103 connected by a 2000 Ω resistor, and equal amounts of overlying water and paddy soil.

104 The experiments were conducted at 25°C. A Raspberry Pi data acquisition system (ARMv7
105 architecture) was connected at both ends of the resistor of CMFC to monitor the voltage. A multimeter
106 was used for verification. The detailed code information can be found in the supplementary material
107 (Section 2). Soil and water samples were taken every 5 days until day 35, and the operation continued
108 for another 10 days until day 45. The electrochemical properties of the SMFC including the polarization
109 curve and power density curve were tested using an electrochemical workstation on days 15 and 30



110 (Ch660e, Shanghai Chenhua Instrument Co., Ltd., Shanghai, China) (Chen et al., 2022b).

111 **2.4 Cr Migration and Transformation**

112 To determine total Cr, 0.50 g soil was subjected to acid digestion (HCl-HNO₃-HClO₄) before
113 measurement using flame atomic absorption spectrometry (FAAS) (PinAAcle 900T AA Spectrometer,
114 PerkinElmer, America). To determine Cr speciation, BCR sequential extraction was applied to divide Cr
115 into HOAc extractable, reducible, oxidizable, and residual fractions with mobility and availability from
116 high to low (Wang et al., 2020a). Also, Cr(VI) concentration in overlying water was determined by a
117 spectrophotometer at 540 nm, while Cr(VI) in soil was determined using FAAS after alkaline digestion
118 (Fan et al., 2021). Duplicates, method blanks, and standard reference materials were used for quality
119 control. Cr recovery in standard reference materials was 92~108%.

120 **2.6 Microbial response during operation**

121 2.6.1 Soil biochemical response

122 Soil dehydrogenase (DHA) activity was measured using 2, 3, 5-triphenyl tetrazolium chloride (TTC)
123 method. Urease activity was determined by the phenol sodium hypochlorite colorimetric assay. Invertase
124 activity was determined by the 3, 5-dinitro salicylic acid colorimetric assay. The acid phosphatase (ACP)
125 activity was determined by the p-nitrophenyl disodium phosphate colorimetric assay (Wang et al., 2019;
126 Wang et al., 2017).

127 2.6.2 Microbial community structure

128 The microbial community structure of the electrodes and soil was determined by high-throughput
129 sequencing. Majorbio (Shanghai, China) performed 16S rRNA gene sequencing using the Illumina HiSeq



130 platform. 0.50 g of fresh homogenized samples were used to extract the total bacterial DNA with a
131 universal DNA Kit (Omega Biotek Inc., USA). After amplification and purification, the V3-V4
132 hypervariable regions of the bacterial 16S rRNA gene were amplified with primer pairs 338F and 806R.
133 After sequencing, the operational taxonomic units (OTUs) with a 97 % similarity cutoff were clustered
134 using UPARSE version 7.1, and chimeric sequences were identified and removed. The taxonomy of each
135 OTU representative sequence was analyzed by RDP Classifier version 2.2 against the 16S rRNA database
136 using a confidence threshold of 0.7. The alpha diversity, beta diversity, microbial community structure
137 change, and environmental factor correlation analysis were conducted. (Wang et al., 2023c)

138 2.6.3 HRG Fluctuation

139 The abundance of HRGs in the surface soil of SMFC and OMFC anode after operation was analyzed
140 using an SYBR Green real-time fluorescence quantitative PCR system (7500, Thermo Fisher, USA)
141 (Wang et al., 2023a). The soil of OMFC was used for comparison. The detected genes included HRGs
142 (*chrA*, *chrB*, *chrR*, *recG*, *nfsA*, *zupT*, *fpvA*) and MGEs (*intI*, *tnpA02*, *tnpA04*, *tnpA05*). The primer
143 sequences are provided in Table S2.

144 2.7 Data analysis

145 The experimental data were evaluated using one-way analysis of variance (ANOVA) based on three
146 tests. The mean values and standard deviations were calculated using SPSS 22.0 software (IBM, USA).
147 A significance level of $P < 0.05$ was considered statistically significant, while $P < 0.01$ was defined as
148 highly statistically significant. Graphs were plotted using Origin 2022 software.



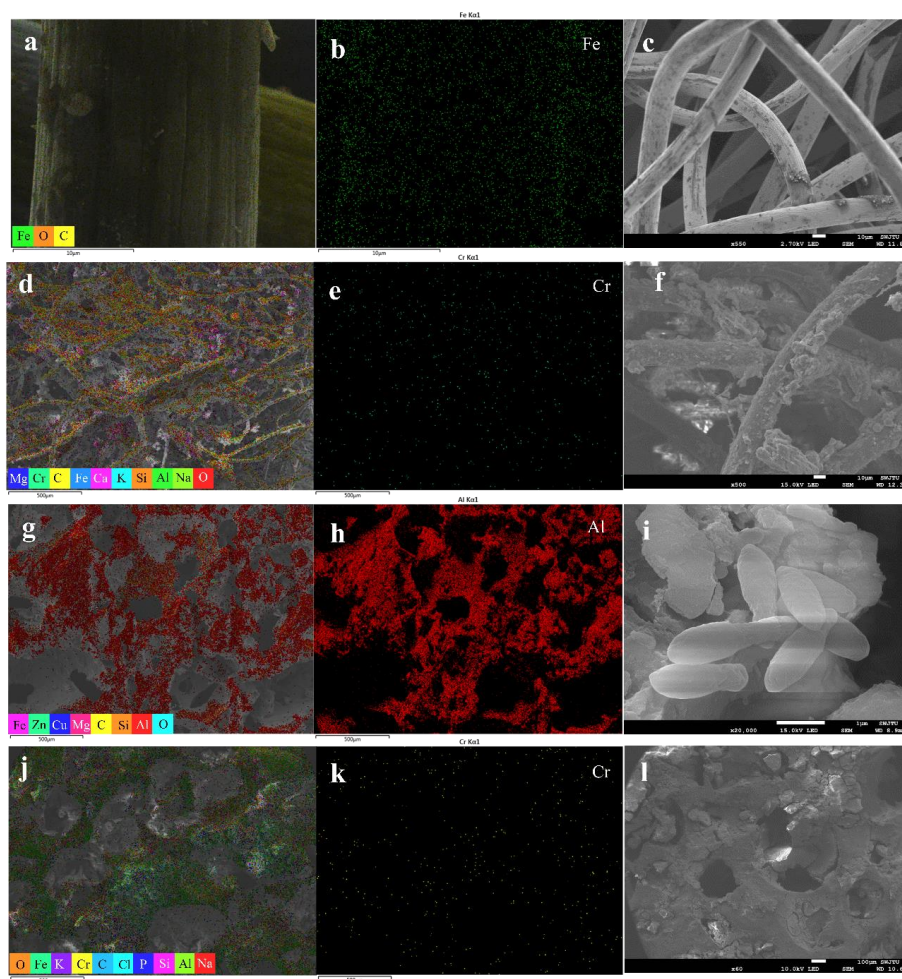
149 **3. Results**

150 **3.1 Electrodes characterization**

151 As demonstrated in Fig. S2, Fig. 1, and Fig. 2, the raw GF had smooth surfaces with C, and O as
152 the main elements (Fig. S2). After Fe₃O₄ loading, black patches constituted with spherical particles
153 appeared, bringing Fe (13.17%) and O (19.97%) on the GF surface (Fig. 1a-c and Table S3). XPS found
154 that peaks of 710.8 and 724.4 eV were consistent with typical Fe₃O₄ peaks (Fig. 2a-b), indicating its
155 successful loading. The CV curves of the cathode (Fig. 2c) presented an obvious oxidation peak at 0.85
156 V, indicating its excellent electrochemical performance.

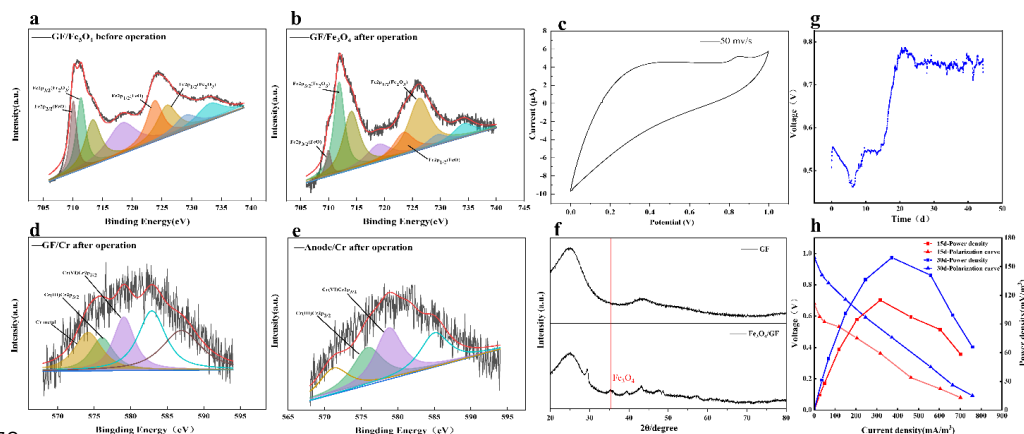
157 After operation, the typical peaks of Cr(III), Cr(VI), and element Cr (576.1 and 578.92) were
158 observed on both electrodes by XPS (Fig. 2d-e), indicating the reduction and immobilization of Cr(VI)
159 by the electrodes. GF was found loaded with many soil elements including Cr, Na, Mg, and Ca (Table
160 S3). SEM also observed many microorganism cells and extracellular organic-like substances, implying
161 the biofilm formation on the cathode (Fig. 1d-f).

162 As presented in Fig. S2C, the raw aluminum foam showed a rough porous structure with mainly Al
163 and O on the surface (Table S3). After loading EAB, many spherical and rod-shaped bacteria were
164 observed, indicating a good capacity to carry microorganisms (Fig. 1g-i). After the operation, many
165 millimeter-scale soil particles were embedded in the anode interspace, indicating the intense mass
166 transfer between the anode and soil (Fig. 1j-l).



167

168 **Fig. 1** Characterization of electrode materials before and after operation by EDS and
169 SEM. (a-c) EDS and SEM images of cathode loaded with Fe_3O_4 ; (d-f) EDS and SEM
170 images of cathode after the SMFC operation; (g-h) EDS and SEM images of anode
171 microorganisms; (j-l) EDS and SEM images of the anode after SMFC operation.



172
173 **Fig. 2** Characterization of electrode materials. (a-b) Fe2p spectra of cathode/Fe₃O₄
174 composite cathode, (c) cyclic voltammetry (CV) curve of cathode/Fe₃O₄, (d-e) Cr2p
175 spectra of GF composite cathode and Anodic Aluminum foam after operation, (f)
176 XRD spectrum of the cathode-Fe₃O₄;
177 Power generation performance of SMFC during long-term operation. (g) output
178 voltage distribution, (h) 15-day vs. 30-day polarization curves and power density
179 curves.

180 3.2 Electricity Generation Performance

181 Initially, CMFC showed a working circuit voltage (WCV) of 0.55 V and an open circuit voltage
182 (OCV) of 0.68 V (Fig. 2g). In the first week, WCV dropped quickly to 0.45 V but bounced back and
183 stabilized at 0.75 V on day 25, implying the adaption process of the anode microbes in the soil.

184 On day 15 (OCV of 0.67 V) and day 30 (OCV of 0.97 V), a series of resistors (50~10 000 Ω) was
185 connected to the electrodes to determine the polarization curves and power density of the SMFC. As
186 shown in Fig. 2h, the power density increased and decreased with the elevation of external resistance. At
187 510 Ω, the power density reached a maximum of 114.9 mW/m³ (73.5 mW/m²) on day 15 and 159.4

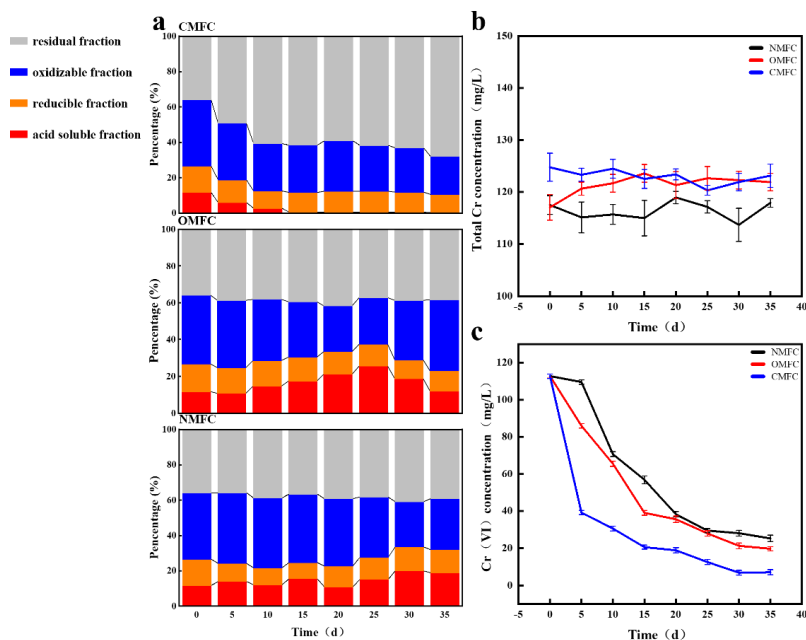


188 mW/m^3 (102.0 mW/m^2) on day 30 (Table S4). The result indicated that the electrochemical performance
189 of SMFC enhanced gradually probably due to the microbial adaption. Even after 45 days, the CMFC still
190 had a WCV of around 0.75 V, indicating its substantial electricity-producing capacity. Compared with
191 the literature, the SMFC in the current work has an outstanding power generation capacity (Table S5).

192 **3.3 Cr(VI) reduction and immobilization during operation**

193 HMs forms determined the bioavailability and toxicity (Jia et al., 2022). After operation, Cr forms
194 in soils were significantly changed ($P<0.05$) (Fig. 3). In CMFC, the acid-soluble Cr decreased
195 substantially by 97.44%, the oxidizable and reducible fractions did not change significantly, while the
196 residual form of Cr increased by 88.89% (Fig. 3a). However, in NMFC, the acid-soluble Cr increased
197 substantially by 61.54% on day 35. In OMFC, the acid-soluble Cr increased before decreasing, which
198 was opposite to its oxidizable state. On day 35, the Cr bioavailability of OMFC (11.9%) and NMFC
199 (18.9%) was 3866-6200 folds of CMFC (0.3%). It is inferred that the electric field and the microbial
200 communities' evolvement may lead to better Cr immobilization.

201 In the meantime, the Cr(VI) concentration (Fig. 3c) dropped in all the groups, and Cr (VI) in
202 CMFC soil was significantly lower than OMFC and NMFC ($P<0.05$) after the experiment. On day 35,
203 CMFC showed 13.59% and 20.87% higher Cr(VI) elimination than OMFC and NMFC, respectively.
204 The overlying water was initially free of Cr. During the experiment (Fig. S3), 0.21~12.72 mg/L Cr was
205 determined, which could be released from the soil. A low level of Cr(VI) (less than 3.15 mg/L) was
206 detected but vanished later (day 15), which could be attributed to the dynamic adsorption-desorption of
207 soil particles and electrodes.



208

209 **Fig. 3** (a) Percentage share of Cr in different chemical fractions in CMFC, OMFC,
210 and NMFC soil; Changes in soil (b) total chromium and (c) Cr(VI) concentrations
211 during SMFC operation.

212 3.4 Soil properties

213 3.4.1 Soil Physicochemical Property

214 The soil pH decreased in all the groups (Fig. S4A). The pH of CMFC decreased fastest from the
215 initial 7.71 to about 6.83 on day 35, with a minimum of 6.77 on day 30, which was 0.14-7.87% lower
216 than others ($P < 0.05$). During the experiment, oxygen in the flooded soil decreased rapidly due to
217 microbial consumption, and acidic products (e.g., low-molecule organic acids) were produced to increase
218 soil acidity. Microorganisms (especially EABs) decompose soil organic matter and release a large



219 number of electrons and protons, making oxidizing substances such as nitrate and high valence metals
220 (Fe(III), Mn(IV), and Cr(VI)) to accept electrons for reduction, causing protons (H^+) accumulation (He
221 et al., 2016). Such a phenomenon was more intense in CMFC due to the rapid electron transfer through
222 wire to the cathode, leaving protons elevated near the anode.

223 In all three groups, EC increased rapidly from the initial 1.55 ms/cm before stabilizing (Fig. S4B),
224 which maximized 2.6, 2.4, and 2.4 ms/cm in CMFC, OMFC, and NMFC ($P>0.05$), respectively. The
225 rapid increase in EC could be attributed to the inundation that increased the soluble salt content of the
226 soils. The electromigration in the MFC electric field may also increase soil mass transfer and positively
227 affect soil electrical conductivity (Zhang et al., 2020).

228 3.4.2 Soil Biochemical Response

229 In all the groups, the DHA activity increased significantly (2 244.0~3 138.0% higher than the initial
230 value) and continuously ($P<0.05$) (Fig. S5A). Under flooding, microbial activity changed from aerobic
231 to anaerobic, leading to a sharp decline in soil redox potential, accompanied by the stimulation of soil
232 DHA (Sardans and Peñuelas, 2005). During operation, urease activity in CMFC showed a gradual
233 increase (2.70~12.40% higher than day 0 from days 10~35), while it in OMFC and NMFC showed a
234 slight decrease (6.10~7.10% lower than day 0 from days 5~35) (Fig. S5B). SMFC electric field and Fe(II)
235 promote extracellular electron transfer (EET) (Chen et al., 2023a), which promotes the enrichment of
236 ammonia-nitrogen transforming bacteria in soil could have caused the higher urease activity in CMFC
237 than NMFC and OMFC ($P<0.05$). Soil invertase activity decreased initially but increased later for CMFC
238 and OMFC, but showed an opposite trend for NMFC. After operation, CMFC had a significantly higher
239 invertase activity than others ($P<0.05$) (Fig. S5C). Soil ACP showed a similar trend with urease, with

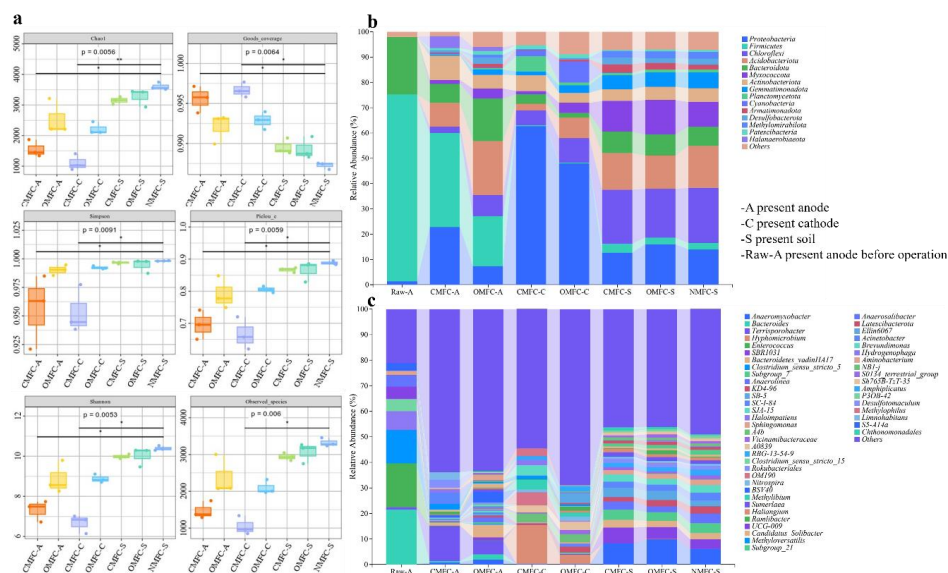


240 CMFC continuously increasing by 13.20–48.90% and considerably higher than OMFC and NMFC (Fig.
241 S5D).

242 **3.5 SMFC operation reshaped soil microbial community**

243 Microbial community structures in the electrodes were analyzed, which obtained 15 dominant phyla
244 and 50 dominant genera (>1.0%). Overall, *Firmicutes* (73.93%), *Proteobacteria* (62.53%), and
245 *Chloroflexi* (21.73%) were found the dominant phyla, while *Bacteroides* (21.48%), *Enterococcus*
246 (17.26%), and *Hyphomicrobium* (15.34%) were the dominant genera.

247 The alpha diversity analysis indicated a significant difference in the microbial community among
248 the samples (Fig. 4a). The higher chao1 index in soils than the electrodes demonstrated the higher
249 microbial richness. Most of the alpha index in OMFC-A and OMFC-C were significantly higher than
250 CMFC-A and CMFC-C, demonstrating a higher microbial richness and diversity in OMFC. The results
251 indicated the different microbial evolution patterns in different electrodes and the selection effect of the
252 electricity field during CMFC operation. The Venn diagram (Fig. S6) found no OTU coincidence among
253 the samples, indicating their obvious specificity. In comparison, 2130 OTUs were shared by CMFC-S,
254 OMFC-S, and NMFC-S, indicating the similarity of the soil microbial community (Fig. S6B). 45 OTUs
255 were shared by Raw-A, CMFC-A, and OMFC-A, accounting for 45.92%, 1.95%, and 1.16%,
256 respectively, indicating the successful colonization and development of the preloaded EABs.



257

258

Fig. 4 (a) Alpha diversity analysis of the electrodes and soils; Microbial

259

community structure is based on (b) the phylum level and (c) the genus level.

260

3.5.1 Soil microbial community reshaping on phylum level

261

Before the operation (Fig. 4b), the anode was dominated by *Firmicutes* (73.93%), *Bacteriodota*

262

(22.74%), and *Proteobacteria* (1.27%). After the operation, *Firmicutes* and *Bacteriodota* decreased by

263

49.83% and 66.84% in CMFC-A, and 73.20% and 26.52% in OMFC-A, respectively. While

264

Proteobacteria increased by 1 698.43% in CMFC-A and 475.59% in OMFC-A. Besides, many other

265

phyla emerged, including *Acidobacteriota* (9.41%~21.40%), *Actinobacteriota* (0.23%~9.52%),

266

Halanaerobiaeota (1.48%~4.77%), *Myxococcota* (1.51%~3.93%), *Chloroflexi* (0.01%~2.57%),

267

probably due to the penetration of soil indigenous microbe.

268

The cathode was free of microorganisms initially. However, many phyla were observed after the

269

operation. The CMFC-C was dominated by *Proteobacteria* (62.53%), *Actinobacteriota* (6.24%),



270 *Planctomycetota* (6.04%), *Chloroflexi* (5.88%), and *Bacteroidota* (3.81%), while OMFC-C was
271 dominated by *Proteobacteria* (47.93%), *Chloroflexi* (9.75%), *Cyanobacteria* (8.30%), *Acidobacteriota*
272 (8.01%), *Actinobacteriota* (3.97%), *Myxococcota* (3.92%), and *Gemmatimonadota* (2.87%). The
273 *Proteobacteria* phylum was rich in EABs, its advantage in both electrodes of CMFC indicated that SMFC
274 operation was favorable for EAB colonization and development. All the soils were dominated by
275 *Chlorobacteria*, *Acidobacteria*, *Proteobacteria*, *Bacteroidetes*, and *Myxococcota*, and the difference was
276 not significant.

277 3.5.2 Soil microbial community reshaping on genus level

278 At the genus level (Fig. 4c), MFC operation presented a selection effect, with *Terrisporobacter*
279 increasing from 0.81% to 13.71% and *Bacteroides* decreasing from 12.48% to 0.53% in CMFC anode.
280 Compared with the Raw-A, many EABs in CMFC-A decreased, including *Clostridium_sensu_stricto_5*
281 (from 12.99% to 0.052%), *Clostridium_sensu_stricto_15* (from 4.70% to 0.47%), *Enterococcus* (from
282 17.26% to 0.03%) (Choi, 2022; Zhang et al., 2023). However, the *Desulfotomaculum* in CMFC-A
283 increased to 3.32% compared with 0.003% in the soil (CMFC-S). Besides, soil indigenous bacteria
284 including *Ramlibacter*, *Methyloversatilis*, and *Acinetobacter* colonized in the anode and elevated by
285 4.89~1 579 fold compared with soil. Nevertheless, multiple dominant genera in the soils decreased in
286 CMFC-A than in OMFC-A. For example, *SBR1031* accounted for 3.63%~6.18% in the soils, but 0.33%
287 in CMFC-A and 1.08% in OMFC-A. *Bacteroidetes_vadinHA17* accounted for 2.48%~3.09% in the soils,
288 but 1.03% in CMFC-A and 5.13% in OMFC-A. *Anaerolinea* accounted for 2.37%~3.63% in the soils,
289 but 0.25% in OMFC-A, and 1.89% in OMFC-A. The electric field action to a certain extent helped the
290 anode to resist external microbial intrusion to ensure the stability of the anodic microbial community.



291 During operation, the prolonged interaction between the soil and water phases resulted in the
292 gradually evolving unique biofilm structure of the cathode. For instance, *Hyphomicrobium* (3.56~15.34%
293 in soils), an aerobic chemoheterotroph capable of degrading a wide range of organics, accounted for
294 15.34% and 3.56% of CMFC-C and OMFC-C, respectively (He et al., 2019). *Hydrogenophaga*, a gram-
295 negative bacteria capable of denitrification and Cr(VI) reduction, accounted for 2.07% of CMFC-C
296 (Wang et al., 2022). Meanwhile, the SMFC operation caused the enrichment of several resistant bacteria.
297 *Subgroup_7*, a typical HM-tolerant bacterium (Li et al., 2023a), was enriched in both cathode and soil.
298 *Acinetobacter* and *Limnohabitans*, also tolerators that carry HRGs and ARGs, were found 4.31% and
299 3.03% in CMFC-A (Dahal et al., 2023; Zhang et al., 2021).

300 The increase of iron in the soil and water due to the use of Fe₃O₄ as the cathode catalyst may be
301 responsible for the enrichment of *Terrisporobacter* and *Anaeromyxobacter* in the CMFC-A and OMFC-
302 A. They were found closely associated with Fe³⁺ reduction to gain energy in various environments (Lin
303 et al., 2007; Wang et al., 2020b).

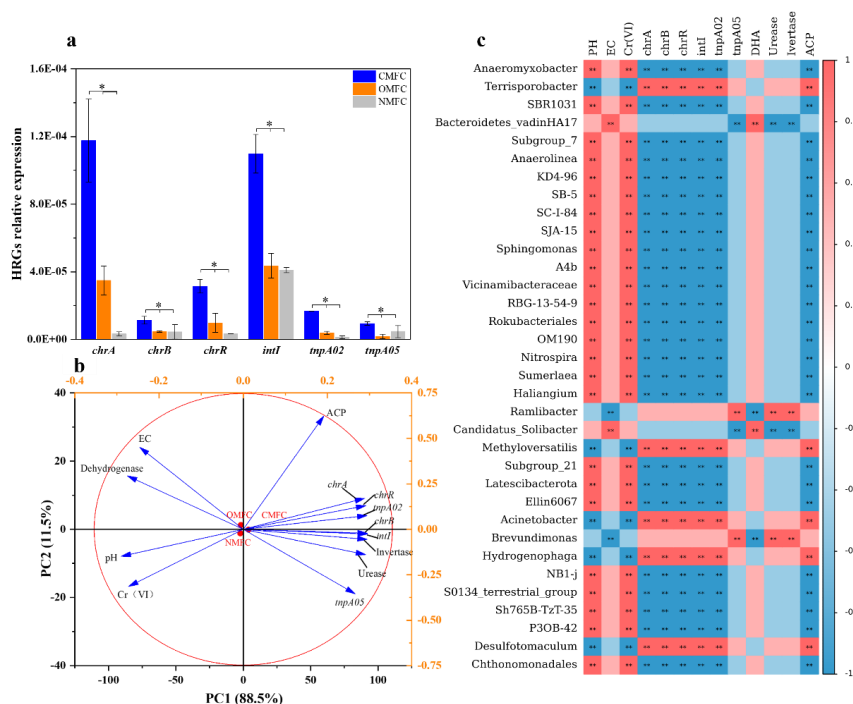
304 3.5.3 Soil metal resistance gene variation

305 Under Cr(VI) stress, certain microbes would utilize pathways like specific or non-specific Cr(VI)
306 reduction, free radical detoxification, DNA damage repair, etc. to survive in toxic environments (Morais
307 et al., 2011). Using qPCR analysis, the abundance of typical HRGs and MGEs in the anodic soils was
308 determined (Fig. 5a), which varied greatly during operation ($P<0.05$). Compared with OMFC and NMFC,
309 *chrA* in CMFC increased by 237.83% and 3414.34%, *chrB* by 141.52% and 153.63%, *chrR* by 221.86%
310 and 839.41%, *IntI* by 151.77% and 167.91%, *tnpA02* by 331.86% and 1118.97%, and *tnpA05* by 416.91%
311 and 99.54%.



312 The elevation of HRGs and MGEs could be due to the enrichment of multiple metal-resistant
313 bacteria (MRB) such as *Acinetobacter*, *Limnohabitans*, and *Brevundimonas*. Moreover, the anodic
314 *Desulfotomaculum*, which accounted for 3.23% of CMFC-A, is a typical sulfate-reducing bacterium
315 (SRB) that produces H₂S, a natural signaling molecule that contributes to tolerance triggering,
316 maintenance, and diffusion through community sensing, which facilitates HRG elevation through HGT
317 (Shatalin et al., 2021). Besides, Cr(VI) reducing bacteria like *Hydrogenophaga* (1.31% in CMFC-A) may
318 also up-regulate the Cr reductase gene *chrR* (Sundarraj et al., 2023).

319 Furthermore, pH changes may also affect soil resistance characteristics. Liu et al. (2023c) observed
320 the abundance of multidrug efflux pump genes in the acid soil was significantly positively correlated
321 with soil acidity. The intensified proton generation and accumulation in CMFC could have led to the
322 HRG elevation. In addition, HMs toxicity exerts direct selective pressure, which affects microbial
323 community structure and their function, leading to the thriving of tolerators like *Desulfotomaculum sp.*,
324 *Hydrogenophaga*, and *Methylophilus* (Hernández-Ramírez et al., 2018), hence the spontaneous HRG
325 elevation(Wang et al., 2023a).



326

327 **Fig. 5** (a)qPCR results of heavy metal resistance gene changes in soil around anode-

328 soil after SMFC operation (*chrA*, *chrB*, *chrR*, *intI*, *tnpA02*, *tnpA05*). Different letters

329 denote significant differences among treatments ($P < 0.05$); (b) principal component

330 analysis (PCA) of SMFC soil physicochemical properties with Enzyme activity,

331 HRGs, and native bacterial genera and (c) Spearman's correlation heatmap (mean

332 relative abundance > 1%). * $P < 0.05$, according to LSD test (mean \pm S.E., $n = 3$);* *

333

$P < 0.01$.

334

335 3.6 Correlation analysis

336 To visually analyze the correlation between bacterial communities and environmental factors,



337 spearman correlation analysis and principal component analysis (PCA) were conducted (Fig. 5b).
338 Spearman correlation analysis (Fig. 5c) isolated four main bacterial genera clusters. Cluster 1
339 (*Terrisporobacter*, *Methyloversatilis*, *Acinetobacter*, *Hydrogenophaga*, and *Desulfotomaculum*) was
340 positively correlated with HRGs (*chrA*, *chrB*, *intI*, *tnpA02*) and ACP ($P<0.01$), but negatively correlated
341 with pH and Cr(VI) ($P<0.01$), suggesting they may contribute to HGT and HRGs enrichment. Cluster 2
342 (*Anaeromyxobacter*, *Subgroup_7*, *Anaerolinea*, *SB-5*, *Sphingomonas*, etc.) was negatively correlated
343 ($P<0.01$) with HRGs (*chrA*, *chrB*, *intI*, *tnpA02*) and ACP, but positively correlated with pH and Cr(VI)
344 ($P<0.01$). Cluster 3 (*Bacteroidetes_vadinHA17* and *Candidatus_Solibacter*) was positively correlated
345 ($P<0.01$) with soil EC and DHA. Cluster 4 (*Ramlibacter*, and *Brevundimonas*) were positively correlated
346 with urease and invertase but negatively correlated with EC.

347 PCA analysis (Fig. 5b) found that soil pH, EC, Cr(VI) concentration, and DHA were positively
348 correlated with each other but negatively correlated with urease, ACP, invertase, and HRGs. Especially,
349 Cr(VI) was significantly negatively correlated with HRGs ($P<0.01$), which could be partially explained
350 by the tolerators thriving and Cr(VI) reduction during SMFC operation.

351 **4. Discussion**

352 In this study, Cr(VI) reduction, microbial community variation, and HRG fate in SMFC were
353 investigated for the first time. The results proved that SMFC was an effective method to eliminate Cr(VI)
354 (93.76%), immobilize Cr (97.44%), and generate electricity (0.97 V).

355 In the SMFC system, Cr(VI) reduction was a synergic result of adsorption/biosorption,
356 bioelectrochemistry reduction, and microbial reduction (Fig. 6). The preloading of Fe_3O_4 and EABs on
357 the electrodes significantly improved Cr(VI) reduction and power generation by accelerating SMFC



358 stabilization. The Cr forms, soil physicochemical properties, soil enzyme activities, and microecological
359 structure mirrored each other, helping to understand Cr transformation patterns and target the key factors
360 affecting metal resistance changes. The detailed explanation is as follows:

361 (1) The electricity-producing process of SMFC can inhibit HMs' release and migration in soil (Feng
362 et al., 2024; Zhu et al., 2019). In this study, Cr forms changed greatly from acid-soluble to a more stable
363 residual fraction. The Fe₃O₄-modified cathode not only directly adsorbs or reduces Cr(VI) due to the high
364 specific area and ferrous iron, but also enhances the electrochemical effect of the system. The electrons
365 derived from anodic microbial metabolism can directly reduce Cr(VI) in the soil to Cr(III), while part of
366 them is transmitted to the cathode, where Cr(VI) in the overlying water compete with oxygen as electron
367 acceptors and complete the current loop (Thapa et al., 2022).

368 (2) Microorganisms can also directly or indirectly reduce or fix Cr. Biosorption, sulfide, and
369 hydroxide precipitation are the main immobilization mechanisms of HMs by microorganisms (Ma et al.,
370 2024). For example, *Desulfotomaculum sp.*, a typical SRB, enriched to 3.23% in CMFC-A, may produce
371 sulfide ions by reducing alienated sulfate, thus forming highly insoluble metal sulfide to fix Cr through
372 microorganism-induced sulfide precipitation (MISP). *Hydrogenophaga*, which dominated in both
373 electrodes, was a known Cr-reducing bacteria. Some iron-reducing bacteria (e.g., *Anaeromyxobacter* and
374 *Terrisporobacter*) may also contribute to Cr(VI) reduction by participating in the Fe cycle through EET,
375 while the ferrous iron reduces Cr(VI). Additionally, the CMFC in this work contains many genera capable
376 of transforming nitrogen. For example, *Hyphomicrobium*, a typical denitrifying bacterium, that can
377 effectively reduce nitrate and nitrite (Ernst et al., 2021), dominated in CMFC-C (15.34%). *Methylophilus*,
378 a methylotrophic microorganism (Yang et al., 2020), accounted for 2.93% of CMFC-A but was much



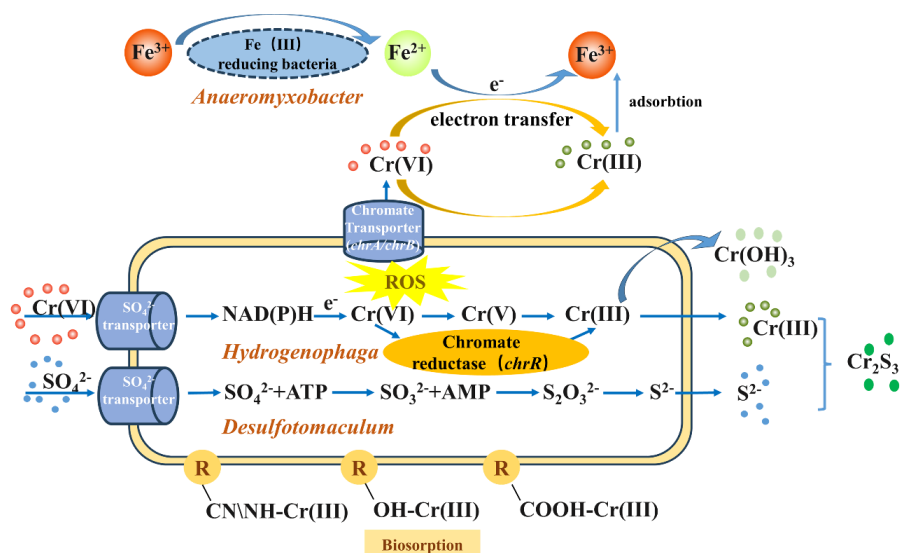
379 lower in other groups. The bacteria mentioned above were found with high urease-producing ability,
380 whose enrichment not only improves soil urease activity and nutrient cycling but also immobilizes Cr
381 through microorganism-induced carbonate precipitation (MICP) (Qian et al., 2017).

382 (3) Under electrochemical selection and HMs stress, the microbial community gradually evolved
383 with higher richness and diversity, along with the HRG enrichment and nutrient cycling variation. Firstly,
384 some soil indigenous bacteria were much lower in CMFC-A than OMFC-A, indicating the electric field
385 contributed to the anode stability by preventing external bacteria intrusion and is less vulnerable to
386 environmental fluctuations. The microbial community change is significantly related to HRG enrichment.
387 Many EABs and MRBs are significantly enriched. For example, *Desulfotomaculum*, an SRB with a dual
388 role of electroproduction and HMs reduction (Jiang et al., 2020; Yin et al., 2021). Other examples also
389 include cumulative-resistant bacteria like *Acinetobacter* and *Limnohabitans* that are only enriched in the
390 CMFC-A (AL-Jabri et al., 2018; Dahal et al., 2023). Their enrichment directly causes vertical gene
391 transfer and HRG elevation.

392 HMs existence in soil can induce HGT occurrence and cause ARG elevation, which has become a
393 major concern (Chen et al., 2023b; Fu et al., 2023). Sub-lethal levels of metal ions can increase mutation
394 rates and enrich de novo mutants with significant resistance to multiple antibiotics (Li et al., 2019). This
395 study focused on the toxic alleviation of a single HM (Cr) in SMFC, during which tolerator accumulation
396 caused considerable HRG enrichment. SMFC is an eco-friendly and cost-effective technology for the in-
397 situ bioremediation of contaminated soil/sediment and powering environmental sensors in remote areas.
398 It has the potential to be used as a novel early warning system for soil environmental hazards.
399 Nevertheless, before the commercialization of large-scale applications in the field, significant efforts



400 should be made to reveal the HRG enrichment mechanism during SMFC operation and pay attention to
 401 ARG change under HMs contamination or HMs-antibiotic co-contamination.



402

403 **Fig. 6** Cr(VI)reduction Mechanism of during SMFC operation

404

405 5. Conclusion

406 During SMFC operation, soil physicochemical properties, enzyme activities, resistance genes, and
 407 microbial community structure closely interacted with each other. The pre-loading of Fe₃O₄ in the
 408 cathode and EAB in the anode greatly contributed to the power production and Cr(VI) elimination.
 409 Anodic microbial metabolism, cathodic redox, and the MFC electric field reduced or immobilized Cr(VI)
 410 to eliminate its risk. The enrichment of multiple MRBs, such as *Acinetobacter*, *Limnohabitans*, and
 411 *Desulfotomaculum*, resulted in HRG elevation, which contributes to microbial adaptation and function
 412 but brings concerns for future application. This study provides a reference for the remediation of HM-
 413 contaminated soil using MFC, which is conducive to promoting the practical application of



414 bioelectrochemical technology in the field.

415 **Author contribution:**

416 Huan Niu: Conceptualization, Investigation, and Writing; Xia Luo: Investigation, Visualization;
417 Peihan Li: Investigation, Visualization; Haitao Ma: Methodology; Hang Qiu: Methodology; Liyue Jiang:
418 Writing-review and editing; Subati Maimaitiali: Writing-review and editing; Minghui Wu: Funding
419 acquisition, Supervision; Fei Xu: Funding acquisition, Supervision; Heng Xu: Funding acquisition,
420 Supervision; Can Wang: Funding acquisition, Supervision.

421 **Acknowledgments**

422 This work was financially supported by the Sichuan Science and Technology Program
423 (2024NSFSC0384), the Government Guides Local Science and Technology Development Project of
424 Tibetan Autonomous Region of China (XZ202401YD0001), the China Postdoctoral Science Foundation
425 (2022M712630), and the Fundamental Research Funds for the Central Universities (2682023ZTPY079).
426 We thank Dr. Weizhen Fang from the Analysis & Testing Center and Dr. Cuijuan Wang from the School
427 of Chemistry, Southwest Jiaotong University, for the technical support. We thank Lijuan Zhang from
428 SCI-Go (www.sci-go.com) for the XPS analysis.

429 **Declaration of interests**

430 The authors declare that they have no known competing financial interests or personal relationships
431 that could have appeared to influence the work reported in this paper.

432 **Reference**

433 AL-Jabri, Z., Zamudio, R., Horvath-Papp, E., Ralph, J.D., AL-Muharrami, Z., Rajakumar, K., Oggioni,
434 M.R., (2018). Integrase-Controlled Excision of Metal-Resistance Genomic Islands in
435 *Acinetobacter baumannii*. *Genes* 9(7), 366. <https://doi.org/10.3390/genes9070366>.



- 436 Chen, C., Fang, Y., Zhou, D., (2023a). Selective pressure of PFOA on microbial community: Enrichment
437 of denitrifiers harboring ARGs and the transfer of ferric-electrons. *Water Research* 233, 119813.
438 <https://doi.org/10.1016/j.watres.2023.119813>.
- 439 Chen, M., Cai, Y., Li, G., Zhao, H., An, T., (2022a). The stress response mechanisms of biofilm formation
440 under sub-lethal photocatalysis. *Applied Catalysis B: Environmental* 307, 121200.
441 <https://doi.org/https://doi.org/10.1016/j.apcatb.2022.121200>.
- 442 Chen, P., Zhang, T., Chen, Y., Ma, H., Wang, Y., Liu, W., Wang, Y., Zhou, G., Qing, R., Zhao, Y., Xu, H.,
443 Hao, L., Wang, C., Xu, F., (2022b). Integrated Chamber-free Microbial Fuel Cell for Wastewater
444 Purification and Bioenergy Generation. *Chemical Engineering Journal*, 136091.
445 <https://doi.org/10.1016/j.ccej.2022.136091>.
- 446 Chen, X., Du, Z., Song, X., Wang, L., Wei, Z., Jia, L., Zhao, R., (2023b). Evaluating the occurrence
447 frequency of horizontal gene transfer induced by different degrees of heavy metal stress. *Journal*
448 *of Cleaner Production* 382, 135371.
449 <https://doi.org/https://doi.org/10.1016/j.jclepro.2022.135371>.
- 450 Choi, S., (2022). Electrogenic Bacteria Promise New Opportunities for Powering, Sensing, and
451 Synthesizing. *Small* 18(18), 2107902. <https://doi.org/10.1002/sml.202107902>.
- 452 Coetzee, J.J., Bansal, N., Chirwa, E.M.N., (2020). Chromium in Environment, Its Toxic Effect from
453 Chromite-Mining and Ferrochrome Industries, and Its Possible Bioremediation. *Exposure and*
454 *Health* 12(1), 51-62. <https://doi.org/10.1007/s12403-018-0284-z>.
- 455 Cong, Y., Shen, L., Wang, B., Cao, J., Pan, Z., Wang, Z., Wang, K., Li, Q., Li, X., (2022). Efficient
456 removal of Cr(VI) at alkaline pHs by sulfite/iodide/UV: Mechanism and modeling. *Water*
457 *Research* 222, 118919. <https://doi.org/10.1016/j.watres.2022.118919>.
- 458 Dahal, U., Paul, K., Gupta, S., (2023). The multifaceted genus *Acinetobacter*: from infection to
459 bioremediation. *Journal of Applied Microbiology* 134(8).
460 <https://doi.org/10.1093/jambio/txad145>.
- 461 Ernst, C., Kayastha, K., Koch, T., Venceslau, S.S., Pereira, I.A.C., Demmer, U., Ermler, U., Dahl, C.,
462 (2021). Structural and spectroscopic characterization of a HdrA-like subunit from
463 *Hyphomicrobium denitrificans*. *The FEBS Journal* 288(5), 1664-1678.
464 <https://doi.org/10.1111/febs.15505>.
- 465 Fan, C., Qian, J., Yang, Y., Sun, H., Song, J., Fan, Y., (2021). Green ceramsite production via calcination
466 of chromium contaminated soil and the toxic Cr(VI) immobilization mechanisms. *Journal of*
467 *Cleaner Production* 315, 128204. <https://doi.org/10.1016/j.jclepro.2021.128204>.
- 468 Fan, Q., Fan, L., Quach, W.-M., Zhang, R., Duan, J., Sand, W., (2023). Application of microbial
469 mineralization technology for marine concrete crack repair: A review. *Journal of Building*
470 *Engineering* 69, 106299. <https://doi.org/10.1016/j.jobe.2023.106299>.
- 471 Feng, H., Jin, A., Yin, X., Hong, Z., Ding, Y., Zhao, N., Chen, Y., Zhang, Y., (2024). Enhancing
472 biocathode denitrification performance with nano-Fe₃O₄ under polarity period reversal.
473 *Environmental Research* 241, 117641. <https://doi.org/10.1016/j.envres.2023.117641>.
- 474 Fu, Y., Zhu, Y., Dong, H., Li, J., Zhang, W., Shao, Y., Shao, Y., (2023). Effects of heavy metals and
475 antibiotics on antibiotic resistance genes and microbial communities in soil. *Process Safety and*
476 *Environmental Protection* 169, 418-427. <https://doi.org/10.1016/j.psep.2022.11.020>.
- 477 Guo, S., Xiao, C., Zhou, N., Chi, R., (2021). Speciation, toxicity, microbial remediation and



- 478 phytoremediation of soil chromium contamination. *Environmental Chemistry Letters* 19(2),
479 1413-1431. <https://doi.org/10.1007/s10311-020-01114-6>.
- 480 Gupta, S., Patro, A., Mittal, Y., Dwivedi, S., Saket, P., Panja, R., Saeed, T., Martínez, F., Yadav, A.K.,
481 (2023). The race between classical microbial fuel cells, sediment-microbial fuel cells, plant-
482 microbial fuel cells, and constructed wetlands-microbial fuel cells: Applications and technology
483 readiness level. *Science of The Total Environment* 879, 162757.
484 <https://doi.org/10.1016/j.scitotenv.2023.162757>.
- 485 Hamdan, H.Z., Salam, D.A., (2023). Sediment microbial fuel cells for bioremediation of pollutants and
486 power generation: a review. *Environmental Chemistry Letters* 21(5), 2761-2787.
487 <https://doi.org/10.1007/s10311-023-01625-y>.
- 488 He, Q., Gui, J., Liu, D., Li, X., Li, P., Quan, S., (2016). Research progress of soil property's changes and
489 its impacts on soil cadmium activity in flooded paddy field. *Journal of Agro-Environment*
490 *Science* 35(12), 2260-2268. <https://doi.org/10.11654/jaes.2016-0892>.
- 491 He, S., Guo, H., He, Z., Yang, C., Yu, T., Chai, Q., Lu, L., (2019). Interaction of *Lolium perenne* and
492 *Hyphomicrobium sp.* GHH enhances the removal of 17 α -ethinyestradiol (EE2) from soil.
493 *Journal of Soils and Sediments* 19(3), 1297-1305. <https://doi.org/10.1007/s11368-018-2116-y>.
- 494 Hernández-Ramírez, K.C., Reyes-Gallegos, R.I., Chávez-Jacobo, V.M., Díaz-Magaña, A., Meza-Carmen,
495 V., Ramírez-Díaz, M.I., (2018). A plasmid-encoded mobile genetic element from *Pseudomonas*
496 *aeruginosa* that confers heavy metal resistance and virulence. *Plasmid* 98, 15-21.
497 <https://doi.org/10.1016/j.plasmid.2018.07.003>.
- 498 Jia, J., Bai, J., Xiao, R., Tian, S., Wang, D., Wang, W., Zhang, G., Cui, H., Zhao, Q., (2022). Fractionation,
499 source, and ecological risk assessment of heavy metals in cropland soils across a 100-year
500 reclamation chronosequence in an estuary, South China. *Science of The Total Environment* 807,
501 151725. <https://doi.org/10.1016/j.scitotenv.2021.151725>.
- 502 Jiang, Y., Shang, Y., Gong, T., Hu, Z., Yang, K., Shao, S., (2020). High concentration of Mn²⁺ has multiple
503 influences on aerobic granular sludge for aniline wastewater treatment. *Chemosphere* 240,
504 124945. <https://doi.org/10.1016/j.chemosphere.2019.124945>.
- 505 Li, C., Huang, H., Gu, X., Zhong, K., Yin, J., Mao, J., Chen, J., Zhang, C., (2023a). Accumulation of
506 heavy metals in rice and the microbial response in a contaminated paddy field. *Journal of Soils*
507 *and Sediments*. <https://doi.org/10.1007/s11368-023-03643-3>.
- 508 Li, X., Gu, A.Z., Zhang, Y., Xie, B., Li, D., Chen, J., (2019). Sub-lethal concentrations of heavy metals
509 induce antibiotic resistance via mutagenesis. *Journal of Hazardous Materials* 369, 9-16.
510 <https://doi.org/10.1016/j.jhazmat.2019.02.006>.
- 511 Li, Y., Chen, Y., Chen, Y., Qing, R., Cao, X., Chen, P., Liu, W., Wang, Y., Zhou, G., Xu, H., Hao, L.,
512 Wang, C., Li, S., Zhu, Y., Haderlein, S., Xu, F., (2023b). Fast deployable real-time bioelectric
513 dissolved oxygen sensor based on a multi-source data fusion approach. *Chemical Engineering*
514 *Journal* 475, 146064. <https://doi.org/10.1016/j.ccej.2023.146064>.
- 515 Lin, B., Hyacinthe, C., Bonneville, S., Braster, M., Van Cappellen, P., Røling, W.F.M., (2007).
516 Phylogenetic and physiological diversity of dissimilatory ferric iron reducers in sediments of
517 the polluted Scheldt estuary, Northwest Europe. *Environmental Microbiology* 9(8), 1956-1968.
518 <https://doi.org/10.1111/j.1462-2920.2007.01312.x>.
- 519 Liu, S., Feng, Y., Li, H., (2023a). Degradation mechanism of saliferous compounding heavy metals-



- 520 organic wastewater by manganese and iron cycling in the microbial fuel cell. Chemical
521 Engineering Journal 473, 145389. <https://doi.org/10.1016/j.cej.2023.145389>.
- 522 Liu, X.-C., Zhang, K.-X., Song, J.-S., Zhou, G.-N., Li, W.-Q., Ding, R.-R., Wang, J., Zheng, X., Wang,
523 G., Mu, Y., (2023b). Tuning Fe₃O₄ for sustainable cathodic heterogeneous electro-Fenton
524 catalysis by acetylated chitosan. Proceedings of the National Academy of Sciences 120(13),
525 e2213480120. <https://doi.org/10.1073/pnas.2213480120>.
- 526 Liu, Z., Zhao, Y., Zhang, B., Wang, J., Zhu, L., Hu, B., (2023c). Deterministic Effect of pH on Shaping
527 Soil Resistome Revealed by Metagenomic Analysis. Environmental Science & Technology
528 57(2), 985-996. <https://doi.org/10.1021/acs.est.2c06684>.
- 529 Ma, S., Mao, S., Shi, J., Zou, J., Zhang, J., Liu, Y., Wang, X., Ma, Z., Yu, C., (2024). Exploring the
530 synergistic interplay of sulfur metabolism and electron transfer in Cr(VI) and Cd(II) removal by
531 *Clostridium thiosulfatireducens*: Genomic and mechanistic insights. Chemosphere 352, 141289.
532 <https://doi.org/10.1016/j.chemosphere.2024.141289>.
- 533 Morais, P.V., Branco, R., Francisco, R., (2011). Chromium resistance strategies and toxicity: what makes
534 *Ochrobactrum tritici 5bvl1* a strain highly resistant. BioMetals 24(3), 401-410.
535 <https://doi.org/10.1007/s10534-011-9446-1>.
- 536 Morales-Benítez, I., Montoro-Leal, P., García-Mesa, J.C., López Guerrero, M.M., Vereda Alonso, E.,
537 (2023). New magnetic chelating sorbent for chromium speciation by magnetic solid phase
538 extraction on-line with inductively coupled plasma optical emission spectrometry. Talanta 256,
539 124262. <https://doi.org/10.1016/j.talanta.2023.124262>.
- 540 Qian, X., Fang, C., Huang, M., Achal, V., (2017). Characterization of fungal-mediated carbonate
541 precipitation in the biomineralization of chromate and lead from an aqueous solution and soil.
542 Journal of Cleaner Production 164, 198-208.
543 <https://doi.org/https://doi.org/10.1016/j.jclepro.2017.06.195>.
- 544 Rani, L., Kaushal, J., Lal Srivastav, A., (2022). Biochar as sustainable adsorbents for chromium ion
545 removal from aqueous environment: a review. Biomass Conversion and Biorefinery.
546 <https://doi.org/10.1007/s13399-022-02784-8>.
- 547 Sardans, J., Peñuelas, J., (2005). Drought decreases soil enzyme activity in a Mediterranean Quercus ilex
548 L. forest. Soil Biology and Biochemistry 37(3), 455-461.
549 <https://doi.org/10.1016/j.soilbio.2004.08.004>.
- 550 Shatalin, K., Nuthanakanti, A., Kaushik, A., Shishov, D., Peselis, A., Shamovsky, I., Pani, B.,
551 Lechpammer, M., Vasilyev, N., Shatalina, E., Rebatchouk, D., Mironov, A., Fedichev, P.,
552 Serganov, A., Nudler, E., (2021). Inhibitors of bacterial H₂S biogenesis targeting antibiotic
553 resistance and tolerance. Science 372(6547), 1169-1175.
554 <https://doi.org/10.1126/science.abd8377>.
- 555 Sundarraj, S., Sudarmani, D.N.P., Samuel, P., Sevakodiyone, S.P., (2023). Bioremediation of hexavalent
556 chromium by transformation of *Escherichia coli DH5a* with chromate reductase (*ChrR*) genes
557 of *Pseudomonas putida* isolated from tannery effluent. Journal of Applied Microbiology 134(1),
558 lxac019. <https://doi.org/10.1093/jambio/lxac019>.
- 559 Thapa, B.S., Kim, T., Pandit, S., Song, Y.E., Afsharian, Y.P., Rahimnejad, M., Kim, J.R., Oh, S.-E., (2022).
560 Overview of electroactive microorganisms and electron transfer mechanisms in microbial
561 electrochemistry. Bioresource Technology 347, 126579.



- 562 <https://doi.org/https://doi.org/10.1016/j.biortech.2021.126579>.
- 563 Wang, C., Jia, Y., Li, J., Li, P., Wang, Y., Yan, F., Wu, M., Fang, W., Xu, F., Qiu, Z., (2023a). Influence
564 of microbial augmentation on contaminated manure composting: metal immobilization, matter
565 transformation, and bacterial response. *J. Hazard. Mater.* 441, 129762.
566 <https://doi.org/https://doi.org/10.1016/j.jhazmat.2022.129762>.
- 567 Wang, C., Jia, Y., Li, J., Wang, Y., Niu, H., Qiu, H., Li, X., Fang, W., Qiu, Z., (2023b). Effect of
568 bioaugmentation on tetracyclines influenced chicken manure composting and antibiotics
569 resistance. *Science of The Total Environment* 867.
570 <https://doi.org/10.1016/j.scitotenv.2023.161457>.
- 571 Wang, C., Jia, Y., Li, J., Wang, Y., Niu, H., Qiu, H., Li, X., Fang, W., Qiu, Z., (2023c). Effect of
572 bioaugmentation on tetracyclines influenced chicken manure composting and antibiotics
573 resistance. *Science of The Total Environment* 867, 161457.
574 <https://doi.org/https://doi.org/10.1016/j.scitotenv.2023.161457>.
- 575 Wang, C., Li, Y.Z., Tan, H., Zhang, A.K., Xie, Y.L., Wu, B., Xu, H., (2019). A novel microbe consortium,
576 nano-visible light photocatalyst and microcapsule system to degrade PAHs. *Chemical
577 Engineering Journal* 359, 1065-1074. <https://doi.org/10.1016/j.cej.2018.11.077>.
- 578 Wang, C., Tan, H., Li, H., Xie, Y., Liu, H., Xu, F., Xu, H., (2020a). Mechanism study of Chromium
579 influenced soil remediated by an uptake-detoxification system using hyperaccumulator, resistant
580 microbe consortium, and nano iron complex. *Environ. Pollut.* 257, 113558.
581 <https://doi.org/10.1016/j.envpol.2019.113558>.
- 582 Wang, C., Zhou, Z., Liu, H., Li, J., Wang, Y., Xu, H., (2017). Application of acclimated sewage sludge
583 as a bio-augmentation/bio-stimulation strategy for remediating chlorpyrifos contamination in
584 soil with/without cadmium. *Science of The Total Environment* 579, 657-666.
585 <https://doi.org/10.1016/j.scitotenv.2016.11.044>.
- 586 Wang, K., Jia, R., Li, L., Jiang, R., Qu, D., (2020b). Community structure of *Anaeromyxobacter* in Fe(III)
587 reducing enriched cultures of paddy soils. *Journal of Soils and Sediments* 20(3), 1621-1631.
588 <https://doi.org/10.1007/s11368-019-02529-7>.
- 589 Wang, Q., Song, X., Wei, C., Jin, P., Chen, X., Tang, Z., Li, K., Ding, X., Fu, H., (2022). In situ
590 remediation of Cr(VI) contaminated groundwater by ZVI-PRB and the corresponding
591 indigenous microbial community responses: a field-scale study. *Science of The Total
592 Environment* 805, 150260. <https://doi.org/10.1016/j.scitotenv.2021.150260>.
- 593 Yaashikaa, P.R., Kumar, P.S., Jeevanantham, S., Saravanan, R., (2022). A review on bioremediation
594 approach for heavy metal detoxification and accumulation in plants. *Environmental Pollution*
595 301, 119035. <https://doi.org/10.1016/j.envpol.2022.119035>.
- 596 Yang, Y., Wang, H., Zheng, Y., Zhu, B., Wu, X., Zhao, F., (2020). Extracellular electron transfer of
597 *Methylophilus methylotrophs*. *Process Biochemistry* 94, 313-318.
598 <https://doi.org/10.1016/j.procbio.2020.05.001>.
- 599 Yin, Y., Chen, Y., Wang, J., (2021). Co-fermentation of sewage sludge and algae and Fe²⁺ addition for
600 enhancing hydrogen production. *International Journal of Hydrogen Energy* 46(13), 8950-8960.
601 <https://doi.org/10.1016/j.ijhydene.2021.01.009>.
- 602 Zhang, J., Liu, Y., Sun, Y., Wang, H., Cao, X., Li, X., (2020). Effect of soil type on heavy metals removal
603 in bioelectrochemical system. *Bioelectrochemistry* 136, 107596.



- 604 <https://doi.org/https://doi.org/10.1016/j.bioelechem.2020.107596>.
- 605 Zhang, Y., Gu, A.Z., Cen, T., Li, X., He, M., Li, D., Chen, J., (2018). Sub-inhibitory concentrations of
606 heavy metals facilitate the horizontal transfer of plasmid-mediated antibiotic resistance genes in
607 water environment. *Environmental Pollution* 237, 74-82.
608 <https://doi.org/10.1016/j.envpol.2018.01.032>.
- 609 Zhang, Y., Shen, G., Hu, S., He, Y., Li, P., Zhang, B., (2021). Deciphering of antibiotic resistance genes
610 (ARGs) and potential abiotic indicators for the emergence of ARGs in an interconnected lake-
611 river-reservoir system. *Journal of Hazardous Materials* 410, 124552.
612 <https://doi.org/10.1016/j.jhazmat.2020.124552>.
- 613 Zhang, Y., Zheng, S., Hao, Q., Wang, O., Liu, F., (2023). Respiratory electrogen *Geobacter* boosts
614 hydrogen production efficiency of fermentative electrotroph *Clostridium pasteurianum*.
615 *Chemical Engineering Journal* 456, 141069. <https://doi.org/10.1016/j.cej.2022.141069>.
- 616 Zhu, J., Zhang, T., Zhu, N., Feng, C., Zhou, S., Dahlgren, R.A., (2019). Bioelectricity generation by
617 wetland plant-sediment microbial fuel cells (P-SMFC) and effects on the transformation and
618 mobility of arsenic and heavy metals in sediment. *Environmental Geochemistry and Health*
619 41(5), 2157-2168. <https://doi.org/10.1007/s10653-019-00266-x>.
- 620